

Low temperature transport in AC-Driven Quantum Dots in the Kondo regime

Rosa Lopez¹, Ramon Aguado², Gloria Platero¹ and Carlos Tejedor³

¹ Teoría de la Materia Condensada, Instituto de Ciencia de Materiales (CSIC)
Cantoblanco, 28049 Madrid, Spain.

² Center for Materials Theory, Department of Physics and Astronomy, Rutgers University,
Piscataway New Jersey 08854-8019, USA

³ Departamento de Física Teórica de la Materia Condensada, Universidad Autónoma de Madrid,
Cantoblanco, 28049 Madrid, Spain.

(April 14, 2024)

Abstract

We present a fully nonequilibrium calculation of the low temperature transport properties of a quantum dot in the Kondo regime when an AC potential is applied to the gate voltage. We solve a time dependent Anderson model with finite on-site Coulomb interaction. The interaction self-energy is calculated up to second order in perturbation theory in the on-site interaction, in the context of the Keldysh non-equilibrium technique, and the effect of the AC voltage is taken into account exactly for all ranges of AC frequencies and AC intensities. The obtained linear conductance and time-averaged density of states of the quantum dot evolve in a non trivial way as a function of the AC frequency and AC intensity of the harmonic modulation..

PACS numbers: 73.40.Gk, 72.15.Qm, 85.30.Vw, 73.50.Mx

I. INTRODUCTION

Recent experiments [1-3] showing Kondo behavior in the low temperature transport of quantum dots (QD's) have opened a new arena for the study of strongly correlated electrons in artificial systems. Kondo effect in dilute magnetic alloys appears as a crossover from weak to strong coupling between delocalized electrons of the host non-magnetic metal and the unpaired localized electron of the magnetic impurity as the temperature (T) is reduced well below the Kondo temperature (T_K) [4]. This crossover leads to the formation of a singlet state between the unpaired localized electron in the impurity and electrons in the host metal.

It is important, however, to emphasize the main differences of the Kondo physics in QD's with respect to bulk magnetic impurities. The parameters which define the T_K in QD's can be changed in a controlled way by applying the appropriate combination of gate voltages. So, it is possible to study either Kondo or Mixed Valence regimes in the same sample. For this to be possible, there is an important requirement: the charging energy and level separation of the QD must be significantly larger than the level broadening due to the coupling to the leads. More importantly, the study of Kondo physics in QD's opens a new road to the study of nonequilibrium many-body phenomena, a relatively young and rich area in contemporary condensed matter physics.

In this paper, we address the issue of a QD driven out of equilibrium by means of an AC voltage. More specifically, we study theoretically the low temperature transport properties of a QD with an AC voltage applied to the central gate. We use a time dependent version of the Anderson model. In its simplest formulation, the Anderson model, valid for both Kondo and Mixed Valence regimes in bulk systems, describes a single discrete level with on-site electron-electron interaction coupled to a band. The model describes different physical regimes which, for QD's, are determined by the following parameters: (i) the energy difference between a discrete level in the QD (ϵ_0) and the Fermi energy of the leads (E_F). (ii) the tunneling coupling (t) between the discrete level in the QD and the electronic states in the

reservoirs. (iii) the QD charging energy (on-site interaction U), i.e., the energy necessary to add an electron to the QD. The relevant energy scale is $T_K = \frac{P}{2U} e^{-\frac{(E_F - \epsilon_0)(U + \epsilon_0)}{2U}}$, which is related to the binding energy of the many body state [4]. For $T < T_K$, the Kondo regime is reached when $\epsilon_0 < E_F$ and $\epsilon_0 > E_F - U +$ and the Mixed Valence regime is established for $E_F - U < \epsilon_0 < E_F$ and $E_F - U < \epsilon_0 < E_F - U +$. In the Kondo regime at $T = 0$, the low energy excitations (quasi-particles) produce a peak at E_F (Kondo resonance or Abrikosov-Suhl resonance) in the density of states (DOS) [4]. One electron at E_F becomes scattered by the QD undergoing a phase shift which is proportional to the displaced charge n (Friedel-Langreth sum rule (FLSR) [5]) and the linear conductance for a QD symmetrically coupled to the leads takes the value $G = (2e^2/h)\sin^2(n)$. In the symmetric case ($\epsilon_0 = -\frac{U}{2}$), $n = 0.5$ leads to a perfect transparency of the QD. For any chemical potential between ϵ_0 and $\epsilon_0 + U$ the QD has the linear conductance as a function of the chemical potential of an almost perfectly open channel $2e^2/h$ [6,8]. However, as temperature increases, inelastic scattering processes reduce the DOS at E_F (i.e., the linear conductance) at the Kondo valley and eventually two peaks at ϵ_0 and $\epsilon_0 + U$ appear for $T \gg T_K$.

As we already mentioned, new questions arise when driving the QD out of equilibrium [9,21]. When this is done by means of the application of a finite DC voltage bias, the linear conductance is reduced and the Kondo peak in the DOS splits [11,14]. More sophisticated configurations of QD's in the Kondo regime constitute a growing area of intense investigations, both from the theoretical and experimental sides. Time dependent Kondo physics [14], Kondo physics in integer-spin QD's [15], QD's embedded in Aharonov-Bohm rings [16] or double QD systems [17], are examples of such configurations.

We focus on the study of the transport properties of an Anderson Hamiltonian with a time dependent resonant level $\epsilon_0(t) = \epsilon_0 + V_{AC} \cos(\omega_0 t)$. This can be achieved experimentally by means of a time dependent central gate voltage capacitively coupled to the QD. In the high temperature regime these type of experiments have indeed been carried out leading to the observation of photon-assisted processes in the Coulomb blockade regime [18,19].

This regime has been studied theoretically as well [20]. In the same way, there has been some theoretical effort devoted to studying the AC transport at very low ($T \ll T_K$) and intermediate temperatures ($T < T_K$) in the Kondo and Mixed Valence regimes [21-27]. Recently transport in an AC driven quantum dot at low temperatures has been measured as well [28].

In this work we clarify the role of an AC voltage in the Kondo effect in QD's. We concentrate on the low temperature regime so that a Fermi liquid theory is adequate in spite of the fact that it overestimates the width of the Kondo peak, i.e., the T_K [4,29]. In fact our Fermi liquid approach gives a resonance width which decreases algebraically with U , instead of having an exponential decay as given by scaling calculations [4]. The occupation of the QD as well as all the relevant quantities in transport have to be calculated by using non-equilibrium propagators. Finally, some approximation is needed for calculating the Green's function of the QD. We use a finite- U perturbation theory for the Green's function of the impurity. The Anderson Hamiltonian is solvable through the Bethe Ansatz [30], Numerical Renormalization Group [31] and Quantum Monte Carlo methods [32] but a reliable and simple method to obtain dynamical properties at low temperatures in the whole range of interactions ($U = \infty$) is not available. Previous efforts have concentrated on the $U \rightarrow \infty$ limit where a Non-Crossing Approximation (NCA) [11,12,21,24] can be made for high and intermediate temperatures. However, such approximations do not give the exact local Fermi liquid properties as $T \rightarrow 0$. They cannot describe the transition from the weak-correlation to the strong-correlation regime. On the other hand, finite- U perturbation theory [9,33,34] describes the symmetric case properly, but presents clear anomalies away from this special situation (which can be overcome by means of an interpolative self-energy [10,25]). In this paper we will restrict ourselves to the symmetric case which is the relevant one for the experimental information available [28]. The study of the asymmetric case will be analyzed elsewhere.

The main difficulty for our purpose resides in the determination of the QD Green's function, and specially of its self-energy. In a previous paper [25] we proposed an ansatz

for the modification of the QD Green's function due to an harmonic modulation. Here, we improve our previous description, valid in the limit of small interaction U , and extend the calculation to finite temperatures.

The paper is organized as follows: in Sec. II we describe the theoretical model and deduce the expressions for the self-energy and the time-averaged spectral density. In Sec. III we present the results for the time-averaged density of states and the linear conductance at finite temperatures and for different AC frequencies and AC intensities of the harmonic modulation. Moreover, we compare with previous experiments and theoretical models. Finally, Sec. IV summarizes the main conclusions of the paper.

II. THEORETICAL MODEL

A. Keldysh Formalism

The application of a time dependent component to the energy level in the Anderson Hamiltonian (See Eq. 6, below) breaks the time translational invariance of the system and, then, we need an approach capable of addressing this fully non-equilibrium situation. When the time dependent perturbation acts for a while, the system does not recover its thermodynamic equilibrium after the perturbation is over. The whole process has not the symmetry between $t \rightarrow -1$ and $t \rightarrow 1$ and, then, it is not possible an equilibrium expansion in terms of expectation values. Nevertheless, the problem can be solved by allowing the system to evolve from -1 to the moment of interest t and then continuously evolve from $t = t$ back to $t \rightarrow -1$. In this way all the expectation values are evaluated in a well-defined state which was prepared in a remote past. This special complex time-contour is the main ingredient of the non-equilibrium Keldysh formalism [35]. By using this complex time-contour (see Fig. 1) the formal expression for the Green's function relative to a total Hamiltonian $H = H_0 + V_{\text{int}}$ which includes an interaction potential V_{int} is given by

$$G_{\alpha\beta}(t;t^0) = i\text{Tr}_C[S(-1;-1)S_+(1;-1)d_{\alpha}(t)d_{\beta}^{\dagger}(t^0)]i; \quad (1)$$

where $S_+(1; 1)$ is the usual S-matrix, $\exp[-i \int_1^{R_1} V_{\text{int}}(t) dt]$ and $S^V(1; 1) = S(1; 1)$. $d(t)$, $d^V(t^0)$ are operators in the interaction picture. $S_+(1; 1)$ depicts the causal branch (from 1 to 1), while $S(1; 1)$ depicts the anticausal branch (from 1 to 1). The Green's function defined in Eq. (1) is a matrix 2×2 , since both times, t and t^0 can belong to the causal branch (causal Green's function, $G_{d;}^C(t; t^0)$) or to the anticausal one (anticausal Green's function, $G_{d;}^C(t; t^0)$) and it is possible to have one time in the causal branch and the other one in the anticausal branch (which defines the lesser, $G_{d;}^<(t; t^0)$ and greater $G_{d;}^>(t; t^0)$ Green's functions). T_c is the contour-ordering operator which arranges the operators on the closed time-path in this way: operators with time labels later on the contour are moved left of operators of earlier time labels. In this way, the non-equilibrium perturbation theory has the same structure as the equilibrium perturbation theory keeping in mind the label of the times. The 2×2 matrix for the Green's function reads

$$G_d(t; t^0) = \begin{matrix} & \begin{matrix} 0 \\ 1 \end{matrix} \\ \begin{matrix} B \\ D \\ A \end{matrix} & \begin{matrix} G_{d;}^C(t; t^0) & G_{d;}^<(t; t^0) \\ G_{d;}^>(t; t^0) & G_{d;}^C(t; t^0) \end{matrix} \end{matrix} \quad (2)$$

where

$$\begin{aligned} G_{d;}^C(t; t^0) &= i T_c d(t) d^V(t^0) g; & G_{d;}^C(t; t^0) &= i T_c d(t) d^V(t^0) g; \\ G_{d;}^<(t; t^0) &= i d^V(t^0) d(t) i; & G_{d;}^>(t; t^0) &= i d(t) d^V(t^0) i; \end{aligned} \quad (3)$$

Here, T is the causal time-ordering operator, and T is the anticausal time-ordering operator. In the conventional Keldysh matrix formulation of the perturbation theory, one does not work directly with the Green's function defined on the complex time-contour, but with a linear combination of these four possible time orders. The usual linear combinations are (similar relations hold for the self-energies)

$$\begin{aligned} G_{d;}^r(t; t^0) &= (t - t^0) [G_{d;}^>(t; t^0) - G_{d;}^<(t; t^0)]; \\ G_{d;}^a(t; t^0) &= (t^0 - t) [G_{d;}^<(t; t^0) - G_{d;}^>(t; t^0)]; \end{aligned} \quad (4)$$

where $G_{d;}^r(t; t^0)$ is the retarded Green's function, $G_{d;}^a(t; t^0)$ is the advanced Green's function, and $G_{d;}^<(t; t^0)$, $G_{d;}^>(t; t^0)$ are the so-called lesser and greater Green's functions, respectively.

B. Hamiltonian

The time dependent Anderson Hamiltonian is:

$$H = H_{\text{leads}} + H_{\text{QD}} + H_{\text{sd}} + H_{\text{AC}}(t); \quad (5)$$

where

$$\begin{aligned} H_{\text{leads}} &= \sum_k c_{k\downarrow}^\dagger c_{k\downarrow} + \sum_k c_{k\uparrow}^\dagger c_{k\uparrow} \\ H_{\text{QD}} &= \epsilon_0 d^\dagger d + U d^\dagger_\uparrow d^\dagger_\downarrow d_\downarrow d_\uparrow \\ H_{\text{sd}} &= \sum_k V_k c_{k\downarrow}^\dagger d + V_k d^\dagger c_{k\uparrow} \\ H_{\text{AC}}(t) &= V_{\text{AC}} \cos(\omega_0 t) d^\dagger d \end{aligned} \quad (6)$$

V_{AC} and ω_0 are the AC intensity and AC frequency of the AC potential respectively. d^\dagger creates an electron with spin \downarrow in the QD, while $c_{k\downarrow}^\dagger$ creates it in the lead with energy ϵ_k (k labels the rest of quantum numbers). The AC voltage modulates in time the relative position of the QD level ϵ_0 with respect to E_F . An eventual breakdown of the spin degeneracy would be represented by $\epsilon_0 \neq \epsilon_{\uparrow 0}$. The coupling V_k between the QD and the leads produces a broadening $\Gamma_{\text{sd}}^{L(R)}(\omega) = 2\text{Im}[\Sigma_{\text{sd}}^{L(R)}(\omega + i0^+)] = 2 \sum_k |V_k|^2 \delta(\omega - \epsilon_k)$, where $\Sigma_{\text{sd}}^{L(R)}$ is the hybridization single-particle self-energy. Hereafter, for simplicity, we consider the wide band (WB) limit approximation which neglects the principal value of the hybridization self-energy and considers the imaginary part to be an energy independent constant, i.e.,

$$\Gamma_{\text{sd}}^{L(R)}(\omega) = \Gamma_{\text{sd}}^{L(R)} = \text{Im}[\Sigma_{\text{sd}}^{L(R)}] = 2 \sum_k |V_k|^2 = 2.$$

C. Model

Here, we discuss the procedure for obtaining the QD Green's functions which allows us to obtain the spectral density of the QD and the linear conductance.

In the remote past, the QD is decoupled from the leads. The coupling between different regions (the contacts and the central region) is treated as a perturbation by means of standard equilibrium perturbation theory. In a first step, the effect of the on-site interaction is

included via a Hartree mean-field approximation (see Appendix A). The time modulation of the QD level is treated via non-equilibrium perturbation theory, since the time translational invariance is broken by the AC voltage. At this point, we include the correlation effects by computing the on-site interaction self-energy (lesser and greater) up to second order by means of the diagrams of Fig. 2. These diagrams are evaluated by using the previous lesser and greater Green's functions as bare propagators (Appendix B). These bare propagators include the coupling between the QD and the contacts, the time dependence of the QD level and the on-site interaction in the Hartree approximation. Once the correlation self-energy has been calculated, the QD retarded Green's function is obtained by means of the time dependent Dyson equation (Eq. 13). Finally, the time-averaged spectral density (Eq. 21) and the linear conductance (Eq. 22) are calculated from the QD retarded Green's function.

D. Correlation self-energy

The starting point for the derivation of the correlation self-energy in the presence of the AC potential, consists of calculating the lesser and greater QD Green's functions, in the Hartree approximation, including coupling to the leads. In the absence of the time dependent potential, the retarded and advanced QD Green's functions have the following expressions (see Appendix A)

$$g_{d;}^{ra}(t-t^0) = -i \langle (t-t^0) \exp \left[i \int_{t^0}^t dt_1 (\epsilon_0 + U n_{d; } - i \Gamma_{2L,R}^P) \right] \rangle; \quad (7)$$

$n_{d; } = \langle d^\dagger(t) d(t) \rangle$ being the QD occupation. Note that these QD Green's functions have been calculated taking into account the coupling self-energy (which is given by $\Gamma_{2L,R}^P$) and the interaction in the Hartree approximation (given by $U n_{d; }$). Now, if one also considers a time modulation of the QD level, the retarded and advanced QD Green's functions have the following forms (see Appendix B)

$$G_{d; }^{ra}(t; t^0) = e^{i \frac{V_{AC}}{\hbar \omega_0} (\sin \omega_0 t - \sin \omega_0 t^0)} g_{d; }^{ra}(t-t^0); \quad (8)$$

The lesser and greater QD Green's functions can be obtained through the wellknown relation [36,37]

$$G_{d;}^{< >}(t; t^0) = \int_{-\infty}^{\infty} dt_1 \int_{-\infty}^{\infty} dt_2 G_{d;}^r(t; t_1) \Sigma_{sd}^{< >}(t_1; t_2) G_{d;}^a(t_2; t^0); \quad (9)$$

where $\Sigma_{sd}^{< >}(t_1; t_2)$ are the lesser and greater coupling self-energies defined in Appendix A (Eqs. A 2 and A 3, respectively). Now we include correlation effects up to second order in the on-site Coulomb interaction (see Fig. 2). The new lesser and greater correlation self-energies are calculated by means of the diagrams of Fig. 2 with bare lines which are given by the propagators of Eq. (9) (analytical expressions are given in Appendix B, Eqs. B 11-B 14):

$$\Sigma_{d;}^{> i(2)}(t; t^0) = iU^2 G_{d;}^>(t; t^0) G_{d;}^{<}(t^0; t) G_{d;}^>(t; t^0); \quad (10)$$

and

$$\Sigma_{d;}^{< i(2)}(t; t^0) = -iU^2 G_{d;}^{<}(t; t^0) G_{d;}^>(t^0; t) G_{d;}^{<}(t; t^0); \quad (11)$$

The retarded self-energy

$$\Sigma_{d;}^{r i(2)}(t; t^0) = (t - t^0) [\Sigma_{d;}^{< i(2)}(t; t^0) - \Sigma_{d;}^{> i(2)}(t; t^0)]; \quad (12)$$

is obtained from Eqs. (10) and (11).

E. Dyson equation

The next step for deriving the retarded QD Green's function consists of solving the retarded time dependent Dyson equation. By using Eq. (12) for the self-energy, one can write

$$i \frac{\partial}{\partial t} G_{d;}(t) = i \int_{-\infty}^{\infty} dt_1 G_{d;}^{r i(2)}(t; t^0) = (t - t^0) + \int_{-\infty}^{\infty} dt_1 \Sigma_{d;}^{r i(2)}(t; t_1) G_{d;}^{r i(2)}(t_1; t^0); \quad (13)$$

where $G_{d;}(t) = G_{d;} + U n_{d;}(t) + V_{AC} \cos \omega_0 t$. Eq. (13) simplifies considerably by making the gauge transformation

$$G_{d;}^{r;(2)}(t;t^0) = -i(t-t^0)e^{i\int_{t^0}^t dt' d(t';t^0)} e^{i\int_{t^0}^t dt' L_R(t')} g(t;t^0); \quad (14)$$

In the presence of time modulation, the retarded Dyson equation becomes

$$\frac{\partial}{\partial t} g(t;t^0) = \int_{t^0}^t dt_1 K(t;t_1) g(t_1;t^0); \quad (15)$$

which is defined only for $t \geq t^0$ due to the θ function appearing in Eq. (14). $K(t;t^0)$ is the kernel of the integro-differential time dependent Dyson equation which is related to the retarded self-energy through the relation:

$$G_{d;}^{r;(2)}(t;t_1) = -i(t-t_1)K(t;t_1) e^{i\int_{t_1}^t dt' d(t';t_1)} e^{i\int_{t_1}^t dt' L_R(t')} g(t;t_1); \quad (16)$$

When $t = t^0$, an additional condition must be imposed in Eq. (13): $G_{d;}^{r;(2)}(t;t) = \langle [f_d(t); d^\dagger(t)g] \rangle = -i$, where fg is the anticommutator. This condition implies that the solution of Eq. (15) when $t = t^0$ is $g(t;t) = 1$.

We solve Eq. (15) by discretizing the temporal variables, the partial derivative is replaced by the finite difference

$$\frac{\partial}{\partial t} g(t;t^0) \rightarrow \frac{g(m;n) - g(m-1;n)}{\Delta t}; \quad (17)$$

where Δt is the grid spacing in time space. The integral is converted into a sum

$$\int_{t^0}^t dt_1 K(t;t_1) g(t_1;t^0) \rightarrow \sum_{k=n}^{X^n} c_k K(m;k) g(k;n); \quad (18)$$

Now, the indexes $m;n$ and k replace the time arguments which appear in the (Eq. 15). The coefficients c_k are equal to 1 except when $m = k$ or $n = k$ in which $c_k = \frac{1}{2}$. In this way, the discretized time dependent Dyson equation has the following form,

$$g(m;n) = g(m-1;n) + \sum_{k=n}^{X^n} c_k K(m;k) g(k;n); \quad (19)$$

Eq. (19) constitutes a set of linear equations that can be solved by standard numerical techniques. Its solution gives the retarded QD Green's function which is used to study the transport properties of the system in the next section.

The time dependent spectral density $\rho(\omega; t)$, being $t = \frac{t+t_0}{2}$, is defined as the imaginary part of the Fourier transform with respect to $\omega = t - t_0$ of the retarded QD Green's function

$$\rho(\omega; t) = -\frac{1}{2} \text{Im} \int_{-\infty}^{\infty} G_{d;1}^{r(2)}(t + \frac{\omega}{2}; t - \frac{\omega}{2}) e^{i\omega t} dt \quad (20)$$

Since the measurement of the linear conductance implies a time-average in t , we work with the time-averaged spectral density which reads

$$\hbar A(\omega) = \frac{1}{2} \int_{-\infty}^{\infty} G_{d;1}^{r(2)}(t + \frac{\omega}{2}; t - \frac{\omega}{2}) e^{i\omega t} dt \quad (21)$$

The linear conductance [36] at finite temperature, in terms of the time-averaged spectral density, is given by

$$G = \frac{e^2}{h} \frac{\Gamma_L \Gamma_R}{\Gamma_L + \Gamma_R} \frac{\partial f(\omega)}{\partial \omega} \hbar A(\omega) \quad (22)$$

where $f(\omega)$ is the Fermi-Dirac distribution function.

III. RESULTS

We solve numerically the set of linear equations (19) for a QD in the Kondo regime (symmetric case $\Gamma_L = \Gamma_R = \Gamma$ with symmetric couplings $\Gamma_L = \Gamma_R = \Gamma$ and $U = 2.5$) and a temperature $T = 0.05$ [38] for different AC frequencies and AC intensities. From the solution of Eq. (19) for the retarded Green's function we obtain the time-averaged density of states (Eq. 21) and the linear conductance (Eq. 22).

The main effect of the AC potential consists in a reduction of the time-averaged DOS at E_F . This reduction can be interpreted as decoherence induced by AC excitations, either by real-photon-assisted induced excitations at large AC frequencies [24] or virtual spin- $\uparrow\downarrow$ cotunneling processes at small AC frequencies [27]. These processes introduce a quenching of the Kondo peak causing a deviation of the linear conductance from the unitary limit. This suppression induced by the AC potential depends on two competing mechanisms regulated

by the AC frequency and by the absorption rate of photons. If the AC frequency is small ($\omega_0 \ll T_K$), a negligible reduction will take place even for a large absorption rate of photons (the probability of absorption depends on Bessel functions with argument $x = V_{AC}/\omega_0$, as shown in appendix B). On the other hand, for large AC frequencies the mechanism of suppression (AC excitations) becomes ineffective as $\omega_0 \gg T_K$.

To analyze in more detail the behavior of the time-averaged DOS as a function of the AC parameters, we plot in Fig. 3 the time-averaged DOS for three different AC frequencies, $\omega_0 = 4T_K$ (Fig. 3a), $\omega_0 = 2T_K$ (Fig. 3b) and $\omega_0 = T_K$ (Fig. 3c). For each AC frequency we consider different AC intensities corresponding to $x = 0, 0.25, 0.5$ and 0.75 . Fig. 3a corresponds to $\omega_0 = 4T_K$ and different AC intensities $V_{AC} = T_K/2$ ($x = 0.25$), $V_{AC} = T_K$ ($x = 0.5$) and $V_{AC} = 3T_K/2$ ($x = 0.75$). In all these situations the Kondo peak is slightly reduced, i. e. the dynamics of the correlated collective state is practically not affected by the AC potentials since both, the AC frequency and the AC intensities are of the order of T_K . Furthermore, there is no evidence of replicas of the Kondo peak in the time-averaged DOS. By doubling ω_0 (Fig. 3b), the Kondo peak undergoes a stronger reduction as the AC intensity grows. In the present case, the two external energy scales, ω_0 and V_{AC} , are larger than T_K yielding to a stronger modification of the time-averaged DOS at E_F . However, a total suppression of the Kondo resonance is only reached for our largest AC frequency (Fig. 3c, $\omega_0 = T_K$). Even for a small value of $x = 0.25$, the Kondo resonance is reduced remarkably. For the highest AC amplitude ($x = 0.75$) the Kondo resonance has been destroyed completely. Another important effect induced by the AC signal in the time-averaged DOS is that the Kondo peak develops satellites. These satellites become apparent in Figs. 3b and 3c. In these cases both ω_0 and V_{AC} are much larger than the relevant energy scale of this problem given by T_K . In Fig. 3c even the second satellites are resolved at $x = 0.5$ [39]. In a mean field model, one should expect an appreciable increase of the satellites of the main peaks in the time-averaged DOS as x increases [40,41]. However, in the present case, the satellites grow very slowly with x due to the two competing mechanisms previously discussed. It is important to note that, the mean field resonances located at ω_0

and $\omega_0 + \frac{U}{2}$ do not display satellites in the time-averaged DOS, since ω_0 is smaller than their widths which are of the order of 2γ .

To illustrate the previous discussion, we plot in Fig. 4 the conductance as a function of V_{AC} for four different AC frequencies. The height of the Kondo peak falls off as the applied AC intensity increases. Moreover, the suppression of the time-averaged DOS at E_F occurs in a very similar way for the low ($\omega_0 = 4$) and intermediate AC frequencies ($\omega_0 = 2, \omega_0 = 1$). This decrease is slower for the largest AC frequency ($\omega_0 = 1.75$), since for each AC amplitude the absorption rate of photons, which depends on ω_0 , is the smallest for the largest AC frequency.

More interesting is the analysis of the conductance as a function of ω_0 , at a fixed AC intensity (in Fig. 5a for $V_{AC} < 0.5$ and in Fig. 6a for $V_{AC} = 0.5$). In both cases we find that there are two regimes separated by a threshold frequency, ω_t , where the conductance has a minimum. The presence of this minimum can be understood, again, by the competition of two opposite effects. In the adiabatic limit, where $\omega_0 \rightarrow 0$, the effect of the applied AC potential has a negligible effect on the dynamics of the correlated collective state. In this case, the quenching of the Kondo peak is no longer effective and, therefore, the AC only induces a small decoherence in the correlated state [27]. In the very high AC frequency limit, where $\omega_0 \rightarrow 1$ (in this limit $\omega_0 \rightarrow 0$), the unpaired electron has a negligible absorption probability. Thus, it is obvious from the previous discussion that the conductance versus ω_0 should display a minimal value. For low AC intensities (Fig. 5a), the threshold frequency depends on the AC amplitude: for $V_{AC} = 0.25$ $\omega_t = 0.5$ and for $V_{AC} = 0.5$ $\omega_t = 0.625$. In both cases, for AC frequencies lower than ω_t the conductance decreases as ω_0 increases whereas this tendency is reversed for AC frequencies larger than ω_t . Note that for $\omega_0 < \omega_t$ the slowest drop of conductance corresponds to the smallest AC amplitude. For $\omega_0 > \omega_t$ the conductance increases with increasing ω_0 . Now, the conductance recovers its undriven limit for smaller AC frequencies in the case of the smallest AC intensity as one should expect. The position of the threshold frequency depends on the competition of the two effects previously

discussed. This competition is illustrated in Fig. 5b, where we plot the time-averaged DOS at E_F for three AC frequencies $\omega_0 = \omega_t$. By increasing the AC frequency from $\omega_0 = 0.375$ up to $\omega_0 = 0.5$ the Kondo resonance is suppressed more effectively than by raising the AC frequency from $\omega_0 = 0.5$ up to $\omega_0 = 0.625$ where the reduction of the Kondo peak is almost negligible. Fig. 6a depicts the conductance vs. ω_0 for $V_{AC} = 1$. Remarkably, if the threshold frequency is normalized to the AC amplitude we find that ω_t decreases extremely slowly for the three AC intensities ($\omega_0 = V_{AC} + 1$). Here, again the suppression of the conductance is slower for the lowest AC amplitude. Furthermore, in the region where the conductance is an increasing function of the AC frequency, this increase is slower for the highest AC intensity. The previous behavior is illustrated in Fig. 6b where we plot the time-averaged DOS for several AC frequencies at the strongest AC intensity $V_{AC} = 2$.

Let us now compare our results with the ones obtained with different schemes [27,24]: Kaminski et al. [27] predict no suppression of the Kondo peak for the symmetric case ($\phi_0 = U=2$) in clear disagreement with both our theory and experimental results [28]. In asymmetric cases, they predict a monotonous decrease of the height of the Kondo peak as a function of ω_0 (in the low AC frequency regime at fixed V_{AC}). Their results (for $\phi_0 \neq U=2$) are similar to our results (for $\phi_0 = U=2$) for AC frequencies below $\omega_0 = 2$ and for low AC intensities (solid line in Fig. 5a) where the Kondo peak is not strongly suppressed. The rest of the cases discussed here are away from the range of validity of Ref. [27].

Using a NCA, Nordlander et al. [24] find a nonmonotonous behavior of the conductance vs. ω_0 and the existence of a minimum, in qualitative agreement with us. Caution is needed, however, in comparing both works due to the different approximations involved and the different regimes of validity for both calculations. Whereas our perturbative calculation is valid for the symmetric case, i. e. particle-hole symmetry, and low temperatures, the NCA considers the limit $U \rightarrow 1$ (i. e. strongly asymmetric case) and temperatures of the order and higher than T_K . In that sense, both calculations should be regarded as complementary. In Fig. 7 we plot the time-averaged DOS at E_F as a function of T in the absence of the AC potential (solid line) and in the presence of the AC potential for $\omega_0 = 1$, $V_{AC} = 0.25$

(dashed line) and $V_{AC} = 0.5$ (dashed line). In the absence of the AC potential, we get the well known strong reduction of the DOS at E_F when the temperature increases, as expected [4]. For the lowest AC intensity case (dotted line) a strong temperature dependence is observed similarly to the case without AC potential (solid line). However, such a dependence changes for the strongest AC intensity (dashed line). In this case, the time-averaged DOS at E_F has been already so strongly reduced at very low temperatures ($T = 0.02$) that an increase of temperature produces only a small further reduction of the linear conductance. This result can be expected for a system where the Kondo effect is already very weak at low temperatures. This behavior of the Kondo peak height as a function of temperature has been confirmed experimentally (Fig. 8 in Ref [28]).

IV . S U M M A R Y

In conclusion, new features are found in the finite temperature transport ($T \ll T_K$) properties of QD's in the Kondo regime as an oscillatory gate voltage is applied. By solving the time dependent Dyson equation we obtain the QD retarded Green's function and the time-averaged density of states within the framework of the Fermi liquid theory. The interaction self-energy in our model is calculated, in the context of the Keldysh non-equilibrium technique, by perturbation theory up to second order in the on-site interaction and the effect of the AC potential is taken into account exactly for all ranges of AC frequencies and AC intensities of the AC potential. The Kondo resonance is modified by the external AC voltage in a different way depending on the range of AC frequencies studied. We find two different AC frequency ranges of opposite behavior, separated by a threshold frequency ω_t where the linear conductance is minimum. ω_t depends on the AC intensity and moves to higher values as V_{AC} increases. At small AC frequencies, and fixed AC intensity, the Kondo peak decreases as ω_0 grows. Once the threshold frequency is reached the opposite behavior is found and the Kondo peak increases as $\omega_0 = \frac{V_{AC}}{\omega_t} \rightarrow 0$. Our results qualitatively agree with previous theories and complete the range of parameters (arbitrary AC frequencies and

AC intensities at finite on-site interaction) and the regime of temperatures (temperatures below T_K). We also analyze the behavior of the Kondo peak as a function of temperature at fixed AC frequency. For large AC intensities, we obtain a very small decrease of the Kondo peak as temperature increases, while for small AC intensities, a much larger quenching of the peak is obtained.

V. ACKNOWLEDGEMENTS

Work supported in part by the MEC of Spain under contracts PB 96-0875, PB 96-0085 and grant PF 98-07497938, the CAM under contract No. 07N/0026/1998; by the NSF grant No. DMR 97-08499 and by the EU via contract FM RX-CT 98-0180. We gratefully acknowledge discussions with David Sanchez and Silvano De Franceschi.

APPENDIX A: QD GREEN'S FUNCTIONS IN THE ABSENCE OF AC POTENTIAL

In this appendix, the QD Green's functions in the absence of time modulation are obtained. First of all, the QD Green's function coupled to the leads is calculated, and afterwards the interaction in the Hartree approximation is included. A very simple calculation yields the exact lesser and greater Green's functions for H_{leads} ,

$$\begin{aligned} g_k^{<,(0)}(t-t^0) &= i h c_k^y(t^0) c_k(t) i = i f(k) e^{i k(t-t^0)}; \\ g_k^{>,(0)}(t-t^0) &= i h c_k(t) c_k^y(t^0) i = i (1 - f(k)) e^{i k(t-t^0)}; \end{aligned} \quad (\text{A } 1)$$

where $f(k)$ is the Fermi-Dirac distribution function. The lesser and greater hopping self-energies including hopping between the QD and the leads are written in terms of the previous Green's functions as [36],

$$\Sigma_{sd}^{<}(t_1-t_2) = \sum_{k \in L,R} V_k g_k^{<}(t_1-t_2) V_k; = i \sum_{L,R}^X \frac{d}{2} e^{i(t_1-t_2)} f_{L=R}(\epsilon) f_{L=R}(\epsilon); \quad (\text{A } 2)$$

$$g_{sd}^{>}(t_1, t_2) = \sum_{k \in L, R} V_k g_k^{>}(t_1, t_2) V_k = i \sum_{L, R}^Z \frac{d}{2} e^{-i(t_1 - t_2)} (1 - f_{L=R}(\epsilon)) \delta_{L=R}(\epsilon) : \quad (A3)$$

where $\delta_{L=R}(\epsilon) = 2 \sum_{k \in L, R}^P \mathcal{V}_k \mathcal{J}^2(\epsilon_k)$ and a similar expression is obtained for $\delta_{L=R}(\epsilon)$. The retarded and advanced self-energies fulfill the relations

$$\begin{aligned} g_{sd}^r(t_1, t_2) &= (t_1 - t_2) (g_{sd}^{>}(t_1, t_2) - g_{sd}^{<}(t_1, t_2)); \\ g_{sd}^a(t_1, t_2) &= (t_2 - t_1) (g_{sd}^{<}(t_1, t_2) - g_{sd}^{>}(t_1, t_2)); \end{aligned} \quad (A4)$$

The Dyson equation for the retarded and advanced QD Green's functions is

$$g_{d;}^{r;a}(t, t^0) = g_{d;}^{r;a;(0)}(t, t^0) + \int_{t_1}^Z \int_{t_2}^Z dt_1 dt_2 g_{d;}^{r;a;(0)}(t, t_1) g_{sd}^{r;a}(t_1, t_2) g_{d;}^{r;a}(t_2, t^0) : \quad (A5)$$

Here $g_{d;}^{r;a;(0)}(t, t^0)$ are the QD Green's functions for H_{QD} (Eq. (6)) without the on-site repulsion term,

$$g_{d;}^{r;a;(0)}(t, t^0) = -i (t - t^0) e^{-i\epsilon_0(t - t^0)} : \quad (A6)$$

In the absence of time dependence, it is advantageous to Fourier transform, getting

$$g_{d;}^{r;a}(\epsilon) = [(g_{d;}^{r;a;(0)})^{-1} - g_{sd}^{r;a}(\epsilon)]^{-1}; \quad (A7)$$

where

$$g_{sd}^{r;a}(\epsilon) = \sum_{k \in L, R} \frac{\mathcal{V}_k \mathcal{J}^2}{\epsilon_k - \epsilon} = \sum_{L, R}^Z (\epsilon) \frac{i}{2} \delta_{L=R}(\epsilon) : \quad (A8)$$

In the W B limit approximation the previous self-energies become $g_{sd}^{r;a}(\epsilon) = \sum_{L, R}^P \frac{i}{2} \delta_{L=R}(\epsilon)$.

By inserting these self-energies in Eq. (A7), the retarded and advanced QD Green's functions coupled to the leads are

$$g_{d;}^{r;a}(\epsilon) = \frac{1}{0; \frac{i}{2} \sum_{L, R}^P} : \quad (A9)$$

One can Fourier transform back to get the time dependence of the retarded and advanced QD Green's functions

$$g_{d;}^{r;a}(t; t^0) = -i (t - t^0) e^{-i \int_{t^0}^t dt_1 (0; \sum_{L, R}^P \delta_{L=R}(\epsilon) = 2)} : \quad (A10)$$

Now the on-site interaction self-energy in the Hartree approximation is calculated via perturbation theory up to first order in U :

$$\Sigma_{d;}^{r;a(1)} = U n_{d;}; \quad (\text{A } 11)$$

where $n_{d;} = \langle d^\dagger(t) d(t) \rangle$. By using the Dyson equation it is straightforward to get

$$g_{d;}^{r;a}(t; t^0) = \frac{1}{i} \langle t - t^0 \rangle e^{i \int_{t^0}^t dt_1 (\epsilon_0 + U n_{d;})} \frac{P}{2L;R} = 2) : \quad (\text{A } 12)$$

APPENDIX B: QD GREEN'S FUNCTIONS IN THE PRESENCE OF AC POTENTIAL

In this appendix the analytical expressions for the lesser and greater QD Green's functions in the presence of an AC potential, coupled to the leads in the Hartree approximation are derived. As we said in Sec. II, one needs to obtain these propagators in order to have an expression of the interaction self-energy which is given by Eq. (12). However, the lesser and greater QD Green's function are given as a function of the retarded and advanced self-energies (see Eq. (9)). Therefore, the first step in this derivation is to compute the retarded and advanced QD Green's functions.

1. retarded and advanced QD Green's Functions

One way to obtain the retarded QD Green's function (similar analysis can be done for the advanced QD Green's function) is by means of perturbation theory in the AC signal up to infinite order. For this purpose, one takes the QD Green's function (A 12) as the bare QD Green's function. Using $\Sigma_{AC}^r(t) = iV_{AC} \cos(\omega_0 t)$ ($\Sigma_{AC}^r(t) = \Sigma_{AC}^c(t) - \Sigma_{AC}^<(t)$, where $\Sigma_{AC}^<(t) = 0$), as the retarded self-energy, the Dyson equation for the retarded QD Green's function reads

$$G_{d;}^r(t; t^0) = g_{d;}^r(t - t^0) + i \int_{t^0}^t dt_1 g_{d;}^r(t - t_1) V_{AC} \cos(\omega_0 t_1) g_{d;}^r(t_1 - t^0) \\ + \frac{1}{2} \int_{t^0}^t dt_1 \int_{t^0}^{t_1} dt_2 g_{d;}^r(t - t_1) V_{AC} \cos(\omega_0 t_1) g_{d;}^r(t_1 - t_2) V_{AC} \cos(\omega_0 t_2) g_{d;}^r(t_2 - t^0) + \dots \quad (\text{B } 1)$$

Eq. (B1) can be written as

$$G_{d;}^r(t; t^0) = g_{d;}^r(t - t^0) - \frac{1}{2} \sum_{p=0}^{\infty} \sum_{m=0}^{\infty} \frac{V_{AC}^p \cos^m(\omega_0 t)}{p! m!} \frac{V_{AC}^m \cos^m(\omega_0 t^0)}{m!} g_{d;}^r(t - t^0) \quad (B2)$$

Performing the summation, one obtains the time dependent retarded QD Green's function:

$$G_{d;}^r(t; t^0) = e^{-i \frac{V_{AC}}{\omega_0} \sin \omega_0 t} e^{-i \frac{V_{AC}}{\omega_0} \sin \omega_0 t^0} g_{d;}^r(t - t^0) = \sum_{p=-\infty}^{\infty} \sum_{m=-\infty}^{\infty} J_m(\frac{V_{AC}}{\omega_0}) J_p(\frac{V_{AC}}{\omega_0}) e^{-ip\omega_0 t} e^{-im\omega_0 t^0} g_{d;}^r(t - t^0) \quad (B3)$$

where $J_m(\cdot)$ is the Bessel function of order m and argument $\frac{V_{AC}}{\omega_0}$. A similar procedure yields the time dependent advanced QD Green's function

$$G_{d;}^a(t; t^0) = e^{-i \frac{V_{AC}}{\omega_0} \sin \omega_0 t} e^{-i \frac{V_{AC}}{\omega_0} \sin \omega_0 t^0} g_{d;}^a(t - t^0) = \sum_{p=-\infty}^{\infty} \sum_{m=-\infty}^{\infty} J_m(\frac{V_{AC}}{\omega_0}) J_p(\frac{V_{AC}}{\omega_0}) e^{-ip\omega_0 t} e^{-im\omega_0 t^0} g_{d;}^a(t - t^0) \quad (B4)$$

2. greater and lesser QD Green's functions

The greater and lesser QD Green's functions are calculated by substituting the retarded and advanced QD Green's functions (Eqs. (B3), (B4)) in Eq. (9):

$$G_{d;}^<(t; t^0) = e^{-i \frac{V_{AC}}{\omega_0} \sin \omega_0 t} e^{-i \frac{V_{AC}}{\omega_0} \sin \omega_0 t^0} \sum_{p=-\infty}^{\infty} \sum_{m=-\infty}^{\infty} J_m(\frac{V_{AC}}{\omega_0}) J_p(\frac{V_{AC}}{\omega_0}) \frac{1}{L} \frac{d}{dt} \frac{e^{ip\omega_0 t} e^{-im\omega_0 t^0} e^{-i(t-t^0)} f_{L=R}(\frac{L}{\omega_0})}{(p! m! \omega_0 + \frac{i}{2}) (m! \omega_0 - \frac{i}{2})}; \quad (B5)$$

$$G_{d;}^>(t; t^0) = e^{-i \frac{V_{AC}}{\omega_0} \sin \omega_0 t} e^{-i \frac{V_{AC}}{\omega_0} \sin \omega_0 t^0} \sum_{p=-\infty}^{\infty} \sum_{m=-\infty}^{\infty} J_m(\frac{V_{AC}}{\omega_0}) J_p(\frac{V_{AC}}{\omega_0}) \frac{1}{L} \frac{d}{dt} \frac{e^{ip\omega_0 t} e^{-im\omega_0 t^0} e^{-i(t-t^0)} (1 - f_{L=R}(\frac{L}{\omega_0}))}{(p! m! \omega_0 + \frac{i}{2}) (m! \omega_0 - \frac{i}{2})}; \quad (B6)$$

$$G_{d;}^<(t^0; t) = e^{-i \frac{V_{AC}}{\omega_0} \sin \omega_0 t} e^{-i \frac{V_{AC}}{\omega_0} \sin \omega_0 t^0} \sum_{p=-\infty}^{\infty} \sum_{m=-\infty}^{\infty} J_m(\frac{V_{AC}}{\omega_0}) J_p(\frac{V_{AC}}{\omega_0}) \frac{1}{L} \frac{d}{dt} \frac{e^{-ip\omega_0 t} e^{im\omega_0 t^0} e^{-i(t^0-t)} f_{L=R}(\frac{L}{\omega_0})}{(p! m! \omega_0 + \frac{i}{2}) (m! \omega_0 - \frac{i}{2})}; \quad (B7)$$

$$G_{d;}^{>}(t^0; t) = e^{i\frac{V_{AC}}{t_0}\sin t_0 t} e^{i\frac{V_{AC}}{t_0}\sin t_0 t^0} \sum_{p=-1}^{X-1} \sum_{m=-1}^{Y-1} J_m(\cdot) J_p(\cdot) \frac{d}{dt} \frac{e^{ip t_0 t} e^{im t_0 t^0} e^{i(t^0 - t)} (1 - f_{L=R}(\cdot))^{L=R}}{(p!_0 \quad 0; + \frac{i}{2} \quad 2L, R) (m!_0 \quad 0; + \frac{i}{2} \quad 2L, R)} : \quad (B8)$$

Once again we have taken $\epsilon_0 = \epsilon_0 + U n_d$, being n_d the QD occupation. In the case of zero DC bias, the right and left Fermi-Dirac distribution functions are $f_{L,R}(\cdot) = \frac{1}{e^{(\epsilon - E_F)/T} + 1}$ where T is the temperature. The analytical expressions for the lesser and greater QD Green's function are obtained by integrating in the complex plane where the Fermi-Dirac distribution function can be written as a difference of two digamma functions which have poles in the lower and upper complex plane:

$$f(z) = \frac{1}{2} = \frac{1}{2i} \left(\frac{1}{2} + \frac{iz}{2T} \right) - \frac{1}{2} \left(\frac{iz}{2T} \right) = \sum_{k=0}^{X-1} \frac{1}{\frac{1}{2} + k + \frac{iz}{2T}} - \frac{1}{\frac{1}{2} + k + \frac{iz}{2T}} : \quad (B9)$$

The complex integrals are performed with the restriction $t - t^0 > 0$ because we use them to evaluate a retarded quantity (the retarded self-energy in Eq. (12)).

In order to abbreviate the notation, we define the following variables

$$\begin{aligned} a_p &= \left(\epsilon_0 + p!_0 + \frac{i}{2} \quad 2L, R \right); b_m = \left(\epsilon_0 + m!_0 + \frac{i}{2} \quad 2L, R \right); \\ p &= \frac{1}{2} + \frac{i}{2T} a_p; m = \frac{1}{2} + \frac{i}{2T} b_m; \quad = e^{-2T(t - t^0)}; \\ u_p &= \frac{1}{2} (1 - \tanh(\frac{1}{2T} a_p)); v_m = \frac{1}{2} (1 - \tanh(\frac{1}{2T} b_m)); \end{aligned} \quad (B10)$$

With this notation, the analytic expressions for the lesser and greater QD Green's functions are:

$$G_{d;}^{>}(t; t^0) = e^{i\frac{V_{AC}}{t_0}\sin t_0 t} e^{i\frac{V_{AC}}{t_0}\sin t_0 t^0} \sum_{p=-1}^{X-1} \sum_{m=-1}^{Y-1} J_m(\cdot) J_p(\cdot) \frac{e^{ip t_0 t} e^{im t_0 t^0}}{(p - m)!_0 \quad i \quad 2L, R} \left(\frac{F_1(p; 1; p + 1;)}{p} - \frac{F_1(m; 1; m + 1;)}{m} \right) 2i(u_p - 1) e^{ia_p(t - t^0)}; \quad (B11)$$

$$G_{d;}^{<}(t; t^0) = e^{i\frac{V_{AC}}{t_0}\sin t_0 t} e^{i\frac{V_{AC}}{t_0}\sin t_0 t^0} \sum_{p=-1}^{X-1} \sum_{m=-1}^{Y-1} J_m(\cdot) J_p(\cdot) \frac{e^{ip t_0 t} e^{im t_0 t^0}}{(p - m)!_0 \quad i \quad 2L, R} \left(\frac{F_1(p; 1; p + 1;)}{p} - \frac{F_1(m; 1; m + 1;)}{m} \right) 2i v_m e^{ib_m(t - t^0)}; \quad (B12)$$

$$G^>(t^0;t) = e^{-i\frac{V_{AC}}{t_0}\sin t_0 t} e^{-i\frac{V_{AC}}{t_0}\sin t_0 t^0} \sum_{p=-1}^{\infty} \sum_{m=-1}^{\infty} J_m(\cdot) J_p(\cdot) \frac{e^{-ip t_0 t} e^{im t_0 t^0}}{(p-m)!_0 i^{\frac{p}{2L_R}}} \left(\frac{F_1(p;1;p+1)}{p} - \frac{F_1(m;1;m+1)}{m} \right) 2iu_p e^{ia_p(t-t^0)}; \quad (B13)$$

$$G^<(t^0;t) = e^{-i\frac{V_{AC}}{t_0}\sin t_0 t} e^{-i\frac{V_{AC}}{t_0}\sin t_0 t^0} \sum_{p=-1}^{\infty} \sum_{m=-1}^{\infty} J_m(\cdot) J_p(\cdot) \frac{e^{-ip t_0 t} e^{im t_0 t^0}}{(p-m)!_0 i^{\frac{p}{2L_R}}} \left(\frac{F_1(p;1;p+1)}{p} - \frac{F_1(m;1;m+1)}{m} \right) 2i(v_m - 1) e^{ib_m(t-t^0)}; \quad (B14)$$

The functions F_1 are hypergeometric functions. Here \cdot and \cdot are complex conjugates of \cdot and \cdot respectively. Once the greater and the lesser QD Green's functions are obtained, the retarded QD interaction self-energy is given by:

$$r_{d;}^{(2)}(t;t^0) = iU^2 (t-t^0) [G_{d;}^<(t;t^0)G_{d;}^>(t^0;t)G_{d;}^<(t;t^0) - G_{d;}^>(t;t^0)G_{d;}^<(t^0;t)G_{d;}^>(t;t^0)]; \quad (B15)$$

Here, we want to point out the non trivial dependence of the retarded self-energy on the parameters of the AC voltage. With this non trivial dependence the QD DOS strongly deviates from the usual single-particle Tien-Gordon behavior. [40,41]

REFERENCES

- [1] D . Goldhaber-Gordon, et al, Nature, 391, 156 (1998); D . Goldhaber-Gordon, et al, Phys.Rev.Lett., 81, 5225 (1998).
- [2] S.M . Cronenwett, Tjerk H . Oosterkamp and Leo.P . Kouwenhoven, Science, 281, 540, (1998).
- [3] J. Schmid, J. Weis, K . Eberl and K . von Klitzing, Physica B , 256-258, 182 (98); J. Schmid, J. Weis, K . Eberl and K . von Klitzing, Phys.Rev.Lett., 84, 5824 (2000).
- [4] A . C . Hewson: The Kondo problem to Heavy Fermions (Cambridge University Press, Cambridge, 1993).
- [5] D . C . Langreth, Phys.Rev. 150, 516 (1966).
- [6] T . K . Ng and P . A . Lee, Phys.Rev.Lett., 61, 1768 (1988).
- [7] L . I . Glazman and M . E . Raikh, JETP Lett., 47, 452 (1988).
- [8] A . Kawabata, J.Phys.Soc.Jpn., 60, 3222 (1991).
- [9] S.Hershfeld, J.H . Davies and J.W . Wilkins, Phys.Rev.Lett., 67, 3720 (1991).
- [10] A . L . Yeyati, A . Mart n-Rodero and F . Flores, Phys.Rev.Lett., 71, 2991 (1993).
- [11] Y . Meir, N . S . Wingreen and P . A . Lee, Phys.Rev.Lett., 70, 2601 (1993).
- [12] N . S . Wingreen and Y . Meir, Phys.Rev.B , 49, 11040 (1994).
- [13] J. König, H . Schoeller and Gerd Schön Phys.Rev.Lett., 76, 1715 (1996); Phys.Rev. B , 54, 16820 (1996).
- [14] M . P lhal, D . C . Langreth and Peter Nordlander, Phys.Rev.B , 61, R13341 (2000); C . Hooley et al, to be published.
- [15] S.Sasaki et al, Nature 405, 764 (2000); M . Eto and Yu.V . Nazarov, Phys.Rev.Lett., 85, 1306 (2000); M . Pustilnik, Y . Avishai, and K . K ikoin, Phys.Rev.Lett. 84, 1756

- (2000); D . Giuliano and A . Tagliacozzo, Phys. Rev. Lett. 84, 4677 (2000); C . Tejedor and L . Martin-Moreno, preprint cond-m at/0003261.
- [16] U . Gerland, J. von Delft, T . Costi and Y . Oreg, Phys. Rev. Lett. 84, 3710 (2000); Yang Ji, et al, preprint cond-m at/0007332.
- [17] T . Ivanov, Europhys. Lett., 40, 183 (1997); T . Pohjola et al, Europhys. Lett., 40, 189 (1997). T . Aono, et al, J. Phys. Soc. Jpn. 67, 1860 (1998); A . Georges and Y . Meir, Phys. Rev. Lett., 82, 3508 (1999); N . Andrei, et al, Phys. Rev. B., 60, R 5125 (1999); Ramon Aguado and David C . Langreth, Phys. Rev. Lett., 85, 1946 (2000); C . A . Busser, et al, cond-m at/9912019; W . Izumida and O . Sakai, cond-m at/9912296.
- [18] L . P . Kouwenhoven, et al, Phys. Rev. Lett., 73, 3443 (1994); T . H . Oosterkamp, et al, Phys. Rev. Lett., 78, 1536 (1997).
- [19] R . H . Blick, et al, Appl. Phys. Lett., 67, 3924 (1995).
- [20] C . Bruder and H . Schoeller, Phys. Rev. Lett., 72, 1076 (1994).
- [21] M . H . Hettler and H . Schoeller, Phys. Rev. Lett., 74, 4907 (1995).
- [22] T . K . Ng, Phys. Rev. Lett., 76, 487 (1996).
- [23] A . Schiller and S . Hershfeld, Phys. Rev. Lett., 77, 1821 (1996).
- [24] P . Nordlander, et al, Phys. Rev. B., 61, 441 (2000).
- [25] Rosa Lopez, Ramon Aguado, Gloria Platero and Carlos Tejedor, Phys. Rev. Lett., 81, 4688, (1998).
- [26] Y . Goldin and Y . Avishai, Phys. Rev. Lett., 81, 5394 (1998); Y . Goldin and Y . Avishai, Phys. Rev. B., 61, 16750 (2000).
- [27] A . Kaminski, Yu V . Nazarov and L . I . Glazman, Phys. Rev. Lett., 83, 384 (1999); *ibid*, cond-m at/0003353.

- [28] Jeroen M. Elzerman et al, *J. Low Temp. Phys.*, 118, 375 (2000).
- [29] P. Nozières, *J. Low Temp. Phys.*, 17, 31 (1974).
- [30] A. M. Tsvelik and P. B. Wiegmann, *Adv. Phys.*, 32, 453 (1983).
- [31] T. A. Costi and A. C. Hewson, *J. Phys. Condens. Matter*, 6, 2519 (1994).
- [32] R. M. Fye and J. E. Hirsch, *Phys. Rev. B*, 38, 433 (1988).
- [33] K. Yosida and K. Yamada, *Prog. Theor. Phys. Suppl.* 46, 224 (1970).
- [34] B. Horvatic and V. Zlatić, *Solid State Commun.* 54, 957 (1985).
- [35] L. V. Keldysh, *Zh. Eksp. Teor. Fiz.* 47, 1515 (1964) [*Sov. Phys. JETP* 20, 1018 (1965)].
- [36] A. P. Jauho, N. S. Wingreen and Y. Meir, *Phys. Rev. B*, 50, 5528 (1994).
- [37] D. C. Langreth, in *Linear and Nonlinear Electron Transport in Solids*, Nato ASI, Series B vol. 17, Ed. J. T. Devreese and V. E. Van Doren (Plenum, New York, 1976).
- [38] As we discuss in the main text, our perturbation scheme in the on-site interaction overestimates T_K . The actual T_K for the parameters we consider can be estimated by using $T_K \sim \frac{P}{2U} e^{-\frac{E_F - \epsilon_j(U + \epsilon_j)}{2U}}$, which gives $T_K \sim 0.12 > T$. Fermi liquid theory is, then, a good approximation to describe the dynamical and transport properties of the QD.
- [39] Note, however, that these satellites can only be observed by measuring the differential conductance $dI = dV_{dc} \frac{d}{dV_{dc}} \rho_{dc} = \rho_0$. The finite dc voltage is an extra source of decoherence, i.e., reduction and broadening of the satellite peaks, [12,27] not addressed here.
- [40] P. K. Tien and J. Gordon, *Phys. Rev.*, 129, 647 (1963).
- [41] Within the Tien and Gordon formalism [40], the time-averaged DOS can be written as: $\rho_p^2(\epsilon) = \rho(\epsilon - p\epsilon_0)$ where, $\rho(\epsilon - p\epsilon_0)$ is the static DOS evaluated at energies given by $p\epsilon_0$ (where p is an integer number). Thus, the single particle time-averaged DOS

shows replicas of the main peaks located at $\omega_i \pm p_0$ (ω_i being the position of the i th main resonance) with a spectral weight proportional to $J_p^2(\omega_i)$ and the main peaks have a spectral weight proportional to $J_0^2(\omega_i)$. This is in contradiction with our observation of a non-trivial dependence of the reduction of the Kondo resonance with ω .

FIGURES

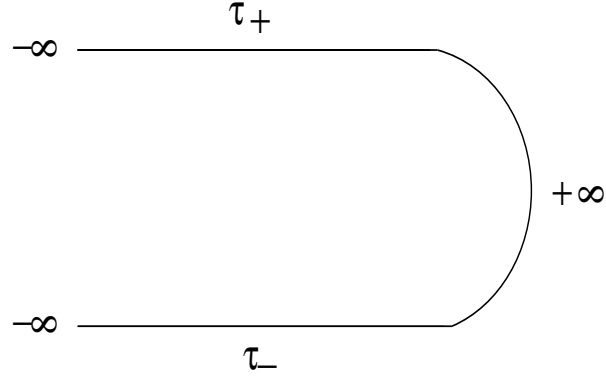


FIG .1. Complex time-contour. The times in the positive branch are τ_+ while times in the negative branch are τ_- .

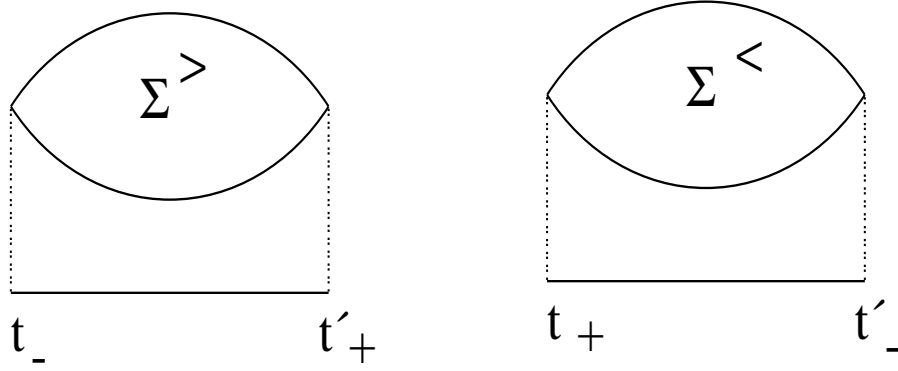


FIG .2. Selfenergies of order U^2 , $\Sigma_d^{> i2}(t; t^0)$ and $\Sigma_d^{< i2}(t; t^0)$. The times in the causal branch are marked with a $+$ symbol whereas the times in the anticausal branch are marked with a $-$ symbol. Solid lines denote QD Green's functions in the Hartree approximation including coupling to the leads and AC potential. Dashed lines correspond to the on-site repulsion U electron-electron interaction.

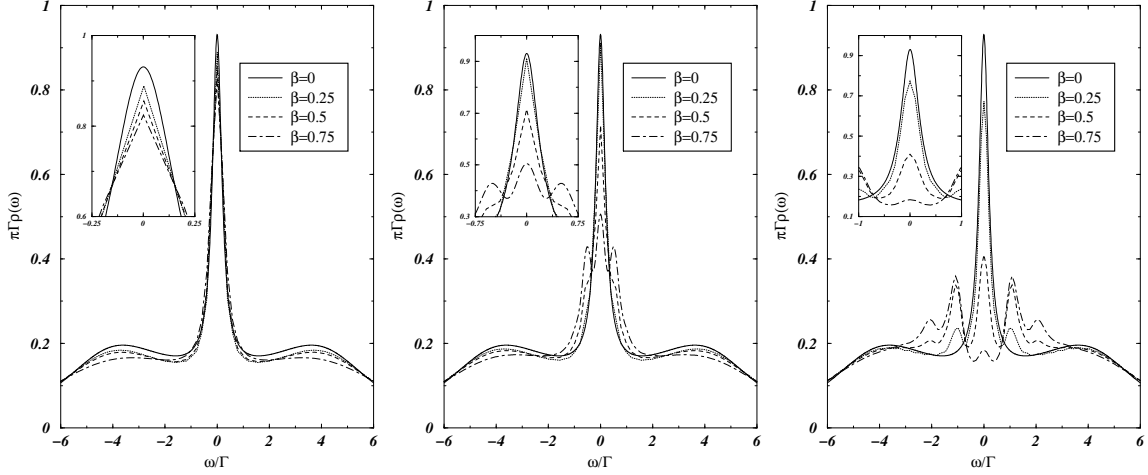


FIG. 3. Time-averaged DOS in the strongly correlated regime, $U = 2.5$ and $T = 0.05$. (a)

The AC frequency is $\omega_0 = -4 - 2T_K$, the solid line is the case in the absence of the AC potential, i.e., $\beta = 0$, where $\beta = \frac{V_{AC}}{\omega_0}$. In this case the peak at E_F reaches a height of 0.93. The dotted line corresponds to $\beta = 0.25$ ($V_{AC} = 0.0625$, $T_K = 2$). The dashed line shows the case of $\beta = 0.5$ ($V_{AC} = 0.125$, T_K). The dot-dashed line corresponds to $\beta = 0.75$ ($V_{AC} = 0.1875$, $3T_K = 2$). In the three cases the Kondo peak is slightly reduced by the AC signal.

(b) $\omega_0 = -2 - 4T_K$. The solid line corresponds to $\beta = 0$, the dotted line to $\beta = 0.25$ ($V_{AC} = 0.125$, T_K). The dashed line shows the case of $\beta = 0.5$ ($V_{AC} = 0.25$, $2T_K$) where the peak has been significantly reduced and the dot-dashed line shows the case of an intense signal where $\beta = 0.75$ ($V_{AC} = 0.375$, $3T_K$). In this case the replicas of the Kondo become apparent (located at ω_0 and $-\omega_0$) and the peak at E_F has been strongly reduced. Figure (c) corresponds to $\omega_0 = 0$: the solid line is for the case $\beta = 0$; the dotted line shows the case $\beta = 0.25$ ($V_{AC} = 0.25$, $2T_K$). At this AC intensity the first satellites of the Kondo resonance show up. The dashed line corresponds to $\beta = 0.5$ ($V_{AC} = 0.5$, $4T_K$), in this case the time-averaged DOS at E_F has been suppressed below 0.5. The dot-dashed line corresponds to a very intense signal, $\beta = 0.75$ ($V_{AC} = 0.75$, $6T_K$), the Kondo peak in this case has completely disappeared. Insets: Blow up of the time-averaged DOS near $\omega = 0$.

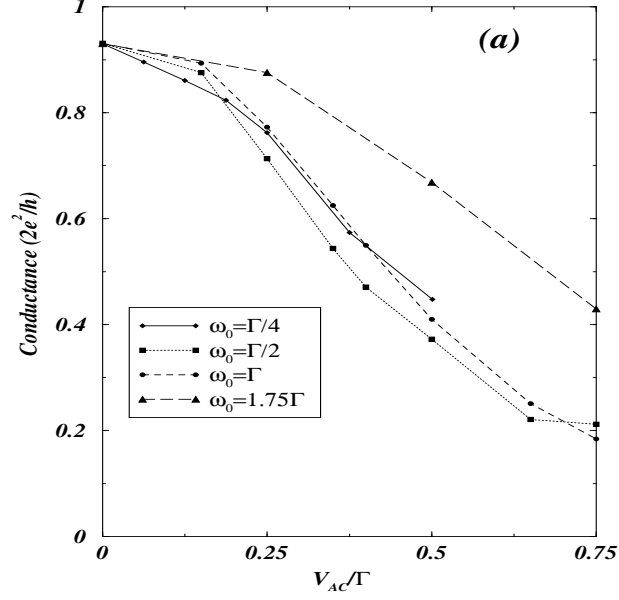


FIG. 4. (a) Conductance as a function of V_{AC} in the correlated regime where, $U = 2.5$ and $T = 0.05$ for four AC frequencies.

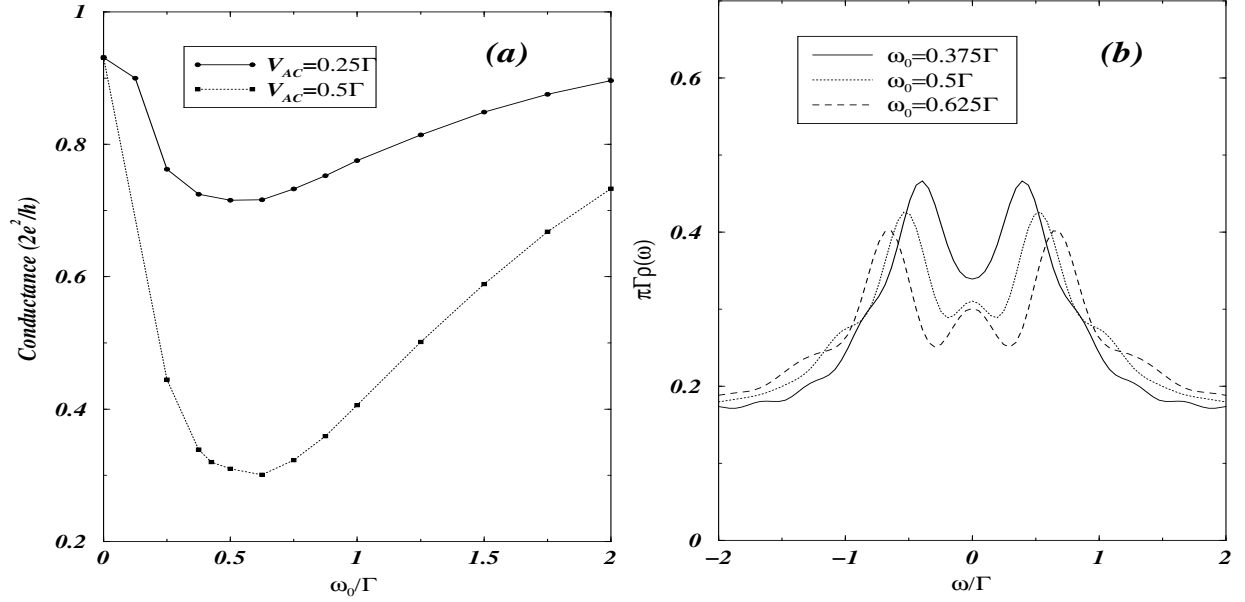


FIG. 5. (a) Conductance as a function of ω_0 in the strong correlated regime $U = 2.5$ and at $T = 0.05$. The solid line shows the case of $V_{AC} = 0.25 \Gamma$, the dotted line corresponds to the case of stronger AC intensity $V_{AC} = 0.5 \Gamma$. (b) Time-averaged DOS for the cases of $\omega_0 = 0.375 \Gamma$ (solid line), $\omega_0 = 0.5 \Gamma$ (dotted line), $\omega_0 = 0.625 \Gamma$ (dashed line) for a fixed AC amplitude $V_{AC} = 0.5 \Gamma$.

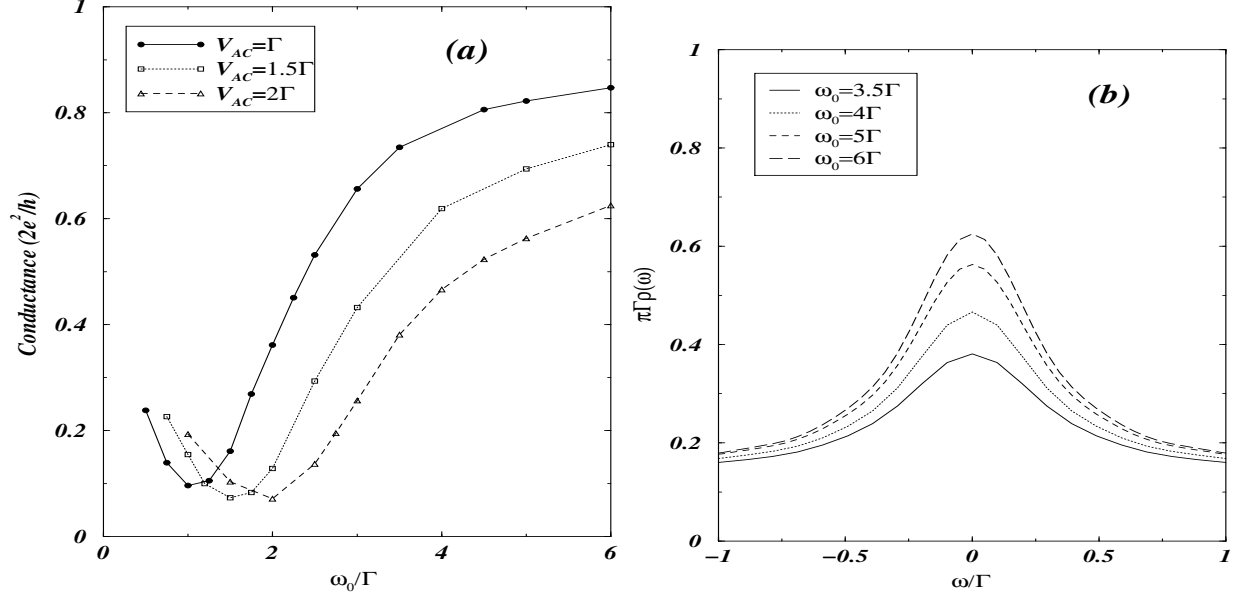


FIG. 6. (a) Conductance as a function of ω_0 in the Kondo regime, $U = 2.5$ and $T = 0.05$.

The solid line shows the case of $V_{AC} = \Gamma$, the dotted line corresponds to the case of $V_{AC} = 1.5$ and dash-dotted line shows the strongest AC intensity $V_{AC} = 2$.

(b) Time-averaged DOS for the strongest field amplitude $V_{AC} = 2$ for different large AC frequencies. The solid line shows the case of $\omega_0 = 3.5$ ($\beta = 0.57$) where the Kondo peak has the lower height, the dotted line shows the case $\omega_0 = 4$ ($\beta = 0.5$), the dashed line corresponds to $\omega_0 = 5$ ($\beta = 0.22$) and the long-dashed line depicts the case of $\omega_0 = 6$ ($\beta = 0.16$).

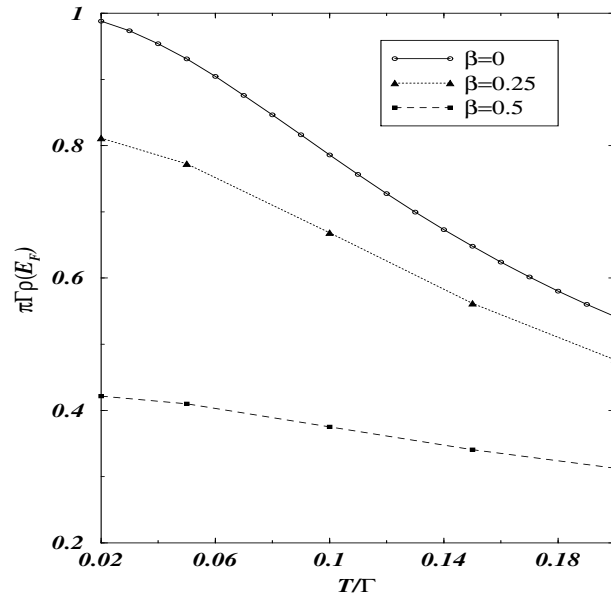


FIG. 7. Time-averaged DOS at E_F for $U = 2.5$ as a function of temperature. The solid line shows the case in the absence of the AC potential. The dotted line corresponds to a case of a low AC intensity $V_{AC} = 0.25$ ($\omega = 0.25$) and the dashed line shows a case with higher AC intensity $V_{AC} = 0.5$ ($\omega = 0.5$). Both of them correspond to an AC frequency $\omega_0 = \omega \gg T_K$.